Distributionally Accurate FMRI Phase Activation

Daniel B. Rowe, Department of Mathematical and Statistical Sciences, Marquette University

John C. Bodenschatz, Department of Mathematical and Statistical Sciences, Marquette University

Abstract

In fMRI, it is important to observe the functioning brain as fast as possible and at as high of a spatial resolution as possible. Increased spatial and temporal speed results in voxels with increased noise relative to signal and contrast. There is much evidence to suggest that there is important biological information contained within the phase component of the fMRI signal. When the signal-to-noise ratio within a voxel is low, as when there is ultra-high resolution, the marginal statistical distribution of the phase is non-standard and difficult to work with. This non-standard marginal phase distribution at high signal-to-noise ratios is normally distributed, but at low signal-to-noise ratios needs to be utilized for accurate modeling.

1. Introduction

Magnetic resonance imaging (MRI) and functional magnetic resonance imaging (fMRI) are continuously increasing spatio-temporal resolution in order to observe the brain greater detail and more rapidly. Increased spatio-temporal resolution in fMRI comes at the cost of a significantly decreased signal-to-noise ratio (SNR) for voxel measurements (Henkelman, 1986; Gudbjartsson and Patz, 1995), making statistical analysis more difficult. The normal distribution generally used for estimation and inferences in fMRI is only valid when the SNR is large.

Historically in fMRI, a general linear model with normally distributed errors was used for the marginal distribution of the magnitude component of the time series (Bandettini et al., 1993). However, the normal assumption is not valid at low SNRs. Recently, efforts have been made to use the proper Ricean marginal distribution for the magnitude component in fMRI (Rowe, 2005; Adrian, Maitra, and Rowe, 2013).

It should be noted that there is also a line of research utilizing the full complex-valued time series (Lai and Glover, 1997, Nan and Nowak, 1999; Rowe and Logan, 2004). In this line of research, task related magnitude, phase, or magnitude and phase activation is computed within the full complex-valued time series. Ever increasing relaxation of the assumed model parameters was made (Adrian, Maitra, and Rowe, 2018; Adrian, Maitra, and Rowe, 2025) as well as Bayesian inference (Yu et al., 2018; Wang et al., 2024).

There has been some effort to estimate and perform inferences on the phase component of the time series. Historically researchers centered each voxel time series, unwrapped it, and simply fit a linear regression model with normally distributed errors. Rowe et al. (Rowe, Meller, and Hoffmann, 2007) approximated Lathi's non-normal marginal distribution (Lathi, 1983) with the von Mises angular distribution (Von Mises, 1918) and an arctangent link function (Johnson and Wehrly 1978) when computing phase-only voxel activation. In this work, phase-only activation will be computed directly from Lathi's mathematically correct non-normal distribution.

2. Methods

2.1 Distributions

It has been well established that that MRI voxel values are complex-valued consisting of real and imaginary parts. The real y_R and imaginary y_I parts of a given voxel value at a specified time contains additive independent and identically distributed normal noise, $y_R \sim N(\rho\cos\theta,\sigma^2)$ and $y_I \sim N(\rho\sin\theta,\sigma^2)$. The bivariate distribution of the real and imaginary parts can be expressed as in Equation 1

$$f(y_R, y_I \mid \rho,\theta,\sigma^2) = \frac{1}{(2\pi\sigma^2)^{1/2}}\exp\left[-\frac{(y_R-\rho\cos\theta)^2}{2\sigma^2}\right]\frac{1}{(2\pi\sigma^2)^{1/2}}\exp\left[-\frac{(y_I-\rho\sin\theta)^2}{2\sigma^2}\right] \tag{1}$$

where the means are coupled by the phase. We can express the complex-valued voxel value in terms of polar coordinates of magnitude and phase. A transformation from Cartesian random variables (y_R,y_I) to polar random variables (r,ϕ), where $y_R=r\cos(\phi)$, $y_I=r\sin(\phi)$ and Jacobian is $J=r$ is performed to arrive at a joint distribution

$$f(r,\phi \mid \rho,\theta,\sigma^2) = \frac{r}{2\pi\sigma^2}\exp\left\{-\frac{1}{2\sigma^2}\left[r^2+\rho^2-2r\rho\cos(\phi-\theta)\right]\right\}. \tag{2}$$

From this bivariate distribution of magnitude and phase in Equation 2, the Ricean marginal distribution for the magnitude with location ρ and scale σ in Equation 3

$$f(r \mid \rho,\sigma^2) = \frac{r}{\sigma^2}\exp\left\{-\frac{r^2+\rho^2}{2\sigma^2}\right\}I_0\left(\frac{r\rho}{\sigma^2}\right) \tag{3}$$

can be derived, where $I_0(\cdot)$ is the modified Bessel function of the first kind with order zero (Rice, 1944; Gudbjartsson and Patz, 1995; Rowe and Logan, 2004). Further, the unnamed non-normal marginal distribution in Equation 4

$$f(\phi \mid \rho,\theta,\sigma^2) = \frac{1}{2\pi}\exp\left[-\frac{\rho^2}{2\sigma^2}\right]\left[1+\frac{\rho}{\sigma}\sqrt{2\pi}\cos(\phi-\theta)\exp\left[\frac{\rho^2\cos^2(\phi-\theta)}{2\sigma^2}\right]\Phi\left(\frac{\rho\cos(\phi-\theta)}{\sigma}\right)\right] \tag{4}$$

for the phase can be found, where $\Phi(\cdot)$ is the cumulative distribution function of the standard normal distribution (Lathi, 1983; Gudbjartsson and Patz, 1995; Rowe and Logan, 2004). Another formulation of the marginal distribution of the phase is

$$f(\phi \mid \rho,\theta,\sigma^2) = \frac{1}{2\pi}\exp\left[-\frac{\rho^2}{2\sigma^2}\right]+\frac{\rho}{\sqrt{2\pi}\sigma}\cos(\phi-\theta)\exp\left[-\frac{\rho^2\sin^2(\phi-\theta)}{2\sigma^2}\right]\Phi\left(\frac{\rho\cos(\phi-\theta)}{\sigma}\right). \tag{5}$$

The mean and variance of the Rice distribution do not have simple forms and involve a Laguerre polynomial. When the true magnitude ρ is zero, the Ricean distribution becomes the Rayleigh distribution with mean $E(r)=\sigma\sqrt{(\pi/2)}$ and variance $E[(r-E(r)])^2=\sigma^2(4-\pi)/2$. When true magnitude ρ is large, it becomes the normal distribution with mean $E(r)=\rho$ and variance σ^2. Generally, $SNR=\rho/\sigma>5$, is considered sufficient for the normal limiting distribution. When the true phase θ is zero, Lathi's non-normal marginal distribution becomes the uniform distribution between $-\pi$ and π and with mean $E(\phi)=0$ and variance $E[(\phi-E(\phi)])^2=\pi^2/3$. When true magnitude ρ is very large, Lathi's marginal non-normal distribution of the phase in Equation 4 becomes the normal distribution with mean $E(\phi)=\theta$ and variance $E[(\phi-E(\phi)])^2=(\sigma/\rho)^2$.

To illustrate these polar marginal distributions, $n=10^6$ random (y_R,y_I) observation pairs were generated from the bivariate distribution in Equation 1 then transformed to polar random variables (r,ϕ) pairs. The true parameter values for the observation pairs are $\rho=2$, $\theta=\pi/6$, and $\sigma^2=3$. The histograms of random observations are presented in Figure 1, magnitude r left and phase ϕ right along with superimposed theoretical distributions. In Figure 1, red vertical lines are true parameter values (and MLEs), the green vertical line is the expectation ($E(r)$ and sample means), and the blue

vertical line is the true median (fiftieth percentile and sample median). Since the phase distribution is circularly symmetric about the center, the true parameter value, median, and mean are the same.

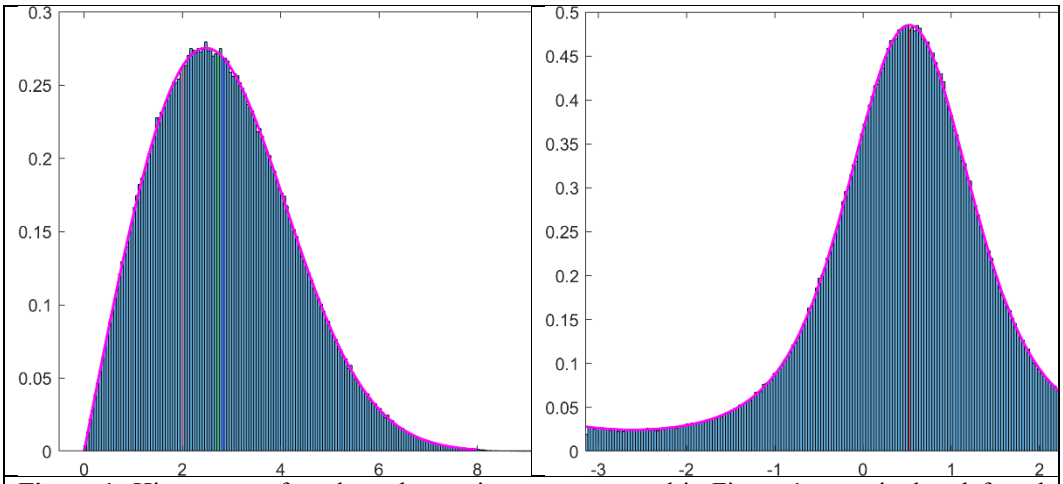

Figure 1: Histograms of random observations are presented in Figure 1, magnitude r left and phase ϕ right along with superimposed theoretical distributions in magenta.

2.2 Estimation

In fMRI, at each voxel location a time series of measurements is taken and an association measure between it and the expected response from the designed experiment is computed. This measure is generally from a linear regression model and applied to the magnitude-only component time-series of the data (Bandettini et al., 1993; Friston et al., 1994). Over the years, the linear model has been expanded to include spatio-temporal correlation such as that induced from processing (Nencka, Hahn, Rowe 2009; Karaman et al. 2014).

Without task, the parameters in Equation 3 can be estimated via maximum likelihood estimation. The likelihood function is

$$L(\rho,\sigma^2)=\prod_{t=1}^{n} f(r_t \mid \rho,\sigma^2)\,, \tag{6}$$

which upon insertion of the Rice distribution becomes

$$L(\rho,\sigma^2)=\prod_{t=1}^{n} \frac{r_t}{\sigma^2}\exp\left\{-\frac{r_i^2+\rho^2}{2\sigma^2}\right\} I_0\left(\frac{r_t\rho}{\sigma^2}\right). \tag{7}$$

Without task, the parameters in Equation 4 can be estimated via maximum likelihood estimation. The likelihood function is

$$L(\rho,\theta_0,\sigma^2)=\prod_{t=1}^{n} f(\phi_t \mid \rho,\theta_0,\sigma^2) \tag{8}$$

where $\theta=\theta_0$ (i.e. $\theta_1=0$) in Equation 4 is the baseline non-task signal.

With task, the parameters in Equation 4 can be estimated via maximum likelihood estimation. The likelihood function is

$$L(\rho,\theta_0,\theta_1,\sigma^2)=\prod_{t=1}^{n} f(\phi_t \mid \rho,\theta_0,\theta_1,\sigma^2) \tag{9}$$

where $\theta_t=\gamma_0+\gamma_1 x_t$ in Equation 4, where γ_0 is the baseline non-task signal, γ_1 is the additive task signal, and x_t is the expected response at time t. Here it is assumed that the magnitude is constant or the *CNR* is small.

Utilizing the distribution in Equation 5 for each of the n observations at time t, the likelihood is

$$L(\rho,\gamma_0,\gamma_1,\sigma^2)=\prod_{t=1}^{n}\left\{\frac{1}{2\pi}\exp\left[-\frac{\rho^2}{2\sigma^2}\right]+\frac{\rho}{\sqrt{2\pi}\sigma}\cos(\phi_t-\theta_t)\exp\left[-\frac{\rho^2\sin^2(\phi_t-\theta_t)}{2\sigma^2}\right]\Phi\left(\frac{\rho\cos(\phi_t-\theta_t)}{\sigma}\right)\right\}. \tag{10}$$

When the null hypothesis is true with $\theta_t=\gamma_0$, the parameters are γ_0 and σ^2, while when the alternative hypothesis is true $\theta_t=\gamma_0+\gamma_1 x_t$ the parameters are γ_0, γ_1, and σ^2. The likelihood for the null and alternative hypotheses can be maximized and the parameters estimated via maximum likelihood. The likelihoods can be maximized with a multitude of optimization methods and the parameters estimated. Here the likelihoods are estimated with a grid search so the likelihood surface can be examined. Since it is well known that the task-related magnitude signal change is extremely small compared to the baseline, an aggregated magnitude MLE $\hat{\rho}$ is estimated using MATLAB's "mle" function and used when computing the phase MLEs from Equation 11.

$$L(\gamma_0,\gamma_1,\sigma^2)=\prod_{t=1}^{n}\left\{\frac{1}{2\pi}\exp\left[-\frac{\hat{\rho}^2}{2\sigma^2}\right]+\frac{\hat{\rho}}{\sqrt{2\pi}\sigma}\cos(\phi_t-\gamma_0-\gamma_1 x_t)\exp\left[-\frac{\hat{\rho}^2\sin^2(\phi_t-\gamma_0-\gamma_1 x_t)}{2\sigma^2}\right]\Phi\left(\frac{\hat{\rho}\cos(\phi_t-\gamma_0-\gamma_1 x_t)}{\sigma}\right)\right\}. \tag{11}$$

A likelihood ratio statistic λ can be computed and the $\Lambda=-2ln(\lambda)\sim\chi^2(1)$ test statistic formed (Wilks, 1938). Since there is a single degree of freedom, a z-statistic

$$z=sign(\hat{\gamma}_1)\sqrt{-2ln(\lambda)} \tag{12}$$

can be utilized (Severini, 2001).

3. Simulation Results

To examine the non-normal marginal phase distribution in a controlled fMRI setting, a single extremely long time series was simulated. The simulated experiment timing was 4096 cycles of 8 s of task and 8 s of non-task resulting in a total of n_t=65536 time points. For the time series, the magnitude and phase varied as $\rho_t=\beta_0+\beta_1 x_t$ and where $\theta_t=\gamma_0+\gamma_1 x_t$ were $\sigma^2=3$, $\beta_0=2$, $SNR=\beta_0/\sigma$, $CNR=1/2$, $\beta_1=CNR\cdot\sigma$, $\theta_0=\pi/6$, and $\theta_1=\pi/36$. Additionally, during task $x_t=1$ and $x_t=0$ during non-task. Histograms of the n_t observations are presented in Figure 2 along with superimposed mixture distributions from Equation 3 and Equation 4 with half of the observations during task ($\rho_t=\beta_0+\beta_1$ and $\theta_t=\gamma_0+\gamma_1$) and half during non-task ($\rho_t=\beta_0$ and $\theta_t=\gamma_0$). The histograms in Figure 2 match the theoretical probability distributions in magenta with a larger sample size.

Maximum likelihood estimates for the magnitude parameters from Equation 7 are $\hat{\rho}=2.3971$ and $\hat{\sigma}^2=3.1379$. Maximum likelihood estimates of the parameters were computed from Equation 11 using a grid search to be $\hat{\theta}_0=0.5050$, $\hat{\theta}_1=0.1134$, $\hat{\sigma}^2=3.0176$ when the alternative hypothesis is true and be $\tilde{\theta}_0=0.5678$, $\tilde{\theta}_1=0$, $\tilde{\sigma}^2=3.0176$ when the null hypothesis is true. Images of the (θ_0,θ_1) likelihood surfaces appeared unimodal for each value of σ^2. These parameter values resulted in likelihood ratio statistics $\Lambda=-2ln(\lambda)=82.5570$ and z-9.0861.

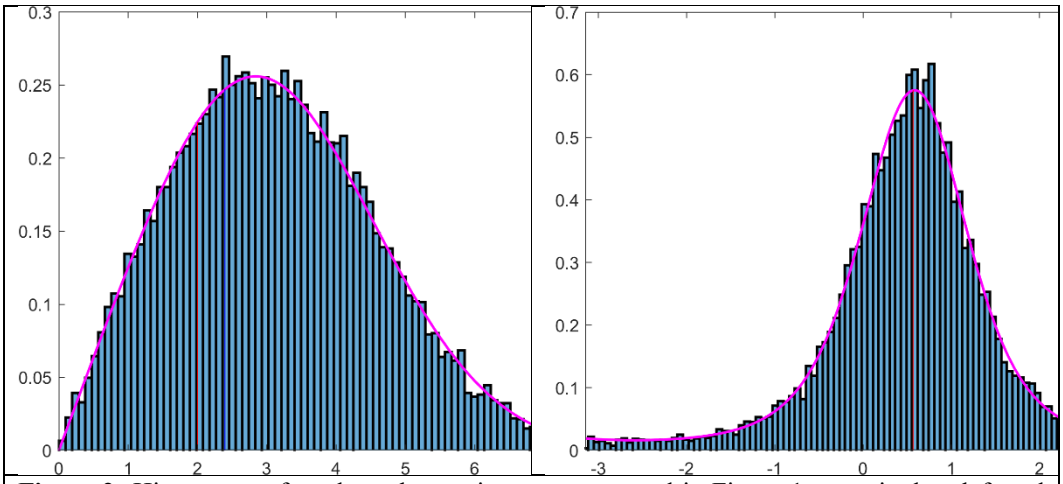

Figure 2: Histograms of random observations are presented in Figure 1, magnitude r left and phase ϕ right along with superimposed theoretical distributions in magenta.

To investigate the statistical properties of the parameter estimates and test statistics, the previous simulation was repeated L=1000 times with 16 cycles of 8 task observations and 8 of non-task observations resulting in a total of n_t=256 time points, which is a typical fMRI time series length.

In Figure 3 are voxel-wise estimates of parameters for each voxel that do not use Equation 5. In Figure 3, we can see that generally all histograms are unimodal and mound shaped. In Figure 3a are the constant maximum likelihood magnitude estimates from Equation 7, In Figure 3b are the maximum likelihood variance estimates for Equation 7. In Figure 3c are $SNR = \hat{\rho}_{Rice} / \hat{\sigma}_{Rice}$ estimates from values in Figure 3a divided by their matched values in Figure 3b. In Figure 3d are the sample angular mean estimated phase values computed by taking each complex value in a time series, dividing it by its magnitude, summing, and computing the resultant's angle. In Figure 3d we can see that the phase value of $\pi/6+\pi/72$=0.5672, baseline phase plus half of the task phase coefficient is in the middle of the histogram. In Figure 3e and Figure 3f are crude estimates of the base phase and task coefficients from an ordinary least squares simple linear regression model. Note

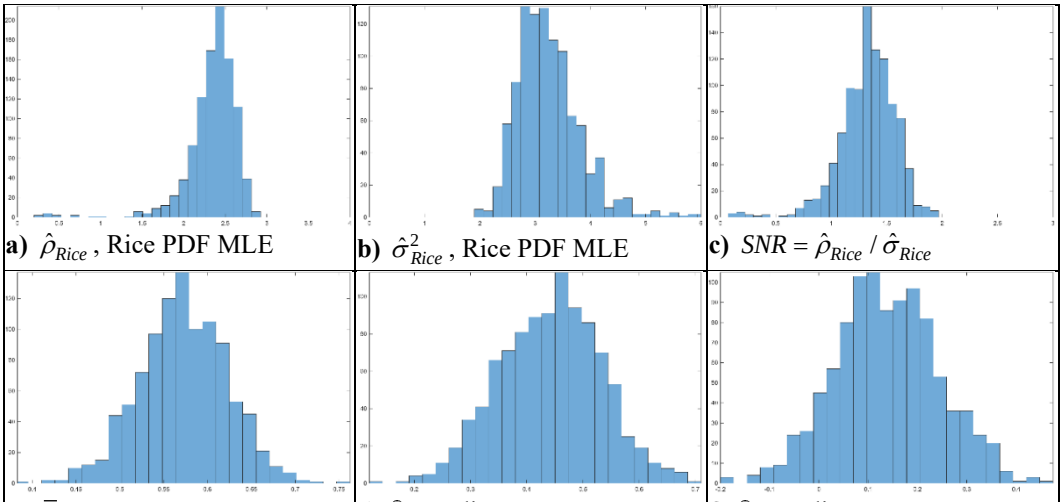

Figure 3: Histograms of simulated data parameter estimates not from phase distribution.

that the simple linear regression estimated baseline and task coefficients in Figures 3e and Figure 3f appear reasonable because the simulated baseline phase was far away from the [-π,π] boundary.

In Figure 5 are voxel-wise estimates of parameters for each voxel that do use Equation 5. In Figure 4a are null hypothesis estimates of the baseline phase coefficient γ_0 from Equation 11. In Figure 4b are null hypothesis estimates of the variance σ^2 from Equation 11. In Figure 4d are alternative hypothesis estimates of the baseline phase coefficient γ_0 from Equation 11. In Figure 4e are alternative hypothesis estimates of the variance σ^2 from Equation 11. In Figure 4c are alternative hypothesis estimates of the task phase coefficient γ_1 from Equation 11. In Figure 4f are signed likelihood ratio test z statistics from Equation 12 for task activation.

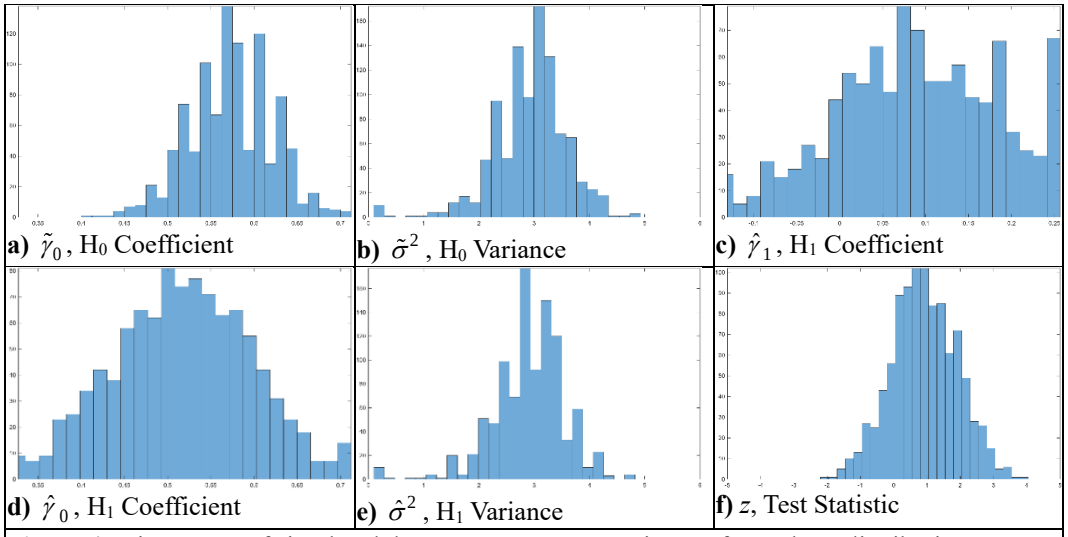

Figure 4: Histograms of simulated data MLE parameter estimates from phase distribution.

From these results, we can see that maximum likelihood parameter estimation from the non-normal phase distribution are accurate at low *SNR*s. Further, activation statistics are accurate and are recommended for use at all *SNR*s.

4. Experimental Results

Experimental data is from a block design right-hand finger tapping experiment on a 3.0-Tesla General Electric Signa LX MRI scanner. The imaging parameters were n_z=7 slices of 2.5 mm thick and 128×128 array size with a field-of-view FOV=24.0 cm, echo time TE=60.4 ms, effective echo spacing EESP=0.832 ms, and time-of-repetition TR= 1 s. The experiment timing followed an initial 16 s of rest followed by 19 epochs of 16 s of task alternating with 16 s of rest resulting in a total of n_t=624 total image volumes. Each slice image at each time point, was Nyquist ghost corrected (Nencka, et al., 2008). Images were phase drift corrected by subtracting each voxel's angular phase temporal mean. A local second order polynomial was spatially fit to the resultant difference of each phase image in the time-series. The spatially fitted phase is angularly subtracted from the original time series (Sakitis and Rowe, 2025). A simple linear regression model was fit to each voxel's unwrapped phase time series and angularly subtracted off. Then the angular mean was added to each voxel's time series, resulting in a linearly stable phase over time.

In Figure 5 are voxel-wise estimates of parameters that do not use Equation 5. In Figure 5a are the constant maximum likelihood magnitude estimates from Equation 7, In Figure 5b are the maximum likelihood variance estimates for Equation 7. In Figure 5c are $SNR = \hat{\rho}_{Rice} / \hat{\sigma}_{Rice}$ estimates from values in Figure 5a divided by their matched values in Figure 5b. In Figure 5d are the sample angular mean estimated phase values computed by taking each complex value in a time series, dividing it by its magnitude, summing, and computing the resultant's angle. In Figure 5e and Figure 5f are crude estimates of the base phase and task coefficients from a simple linear regression model. Note that the simple linear regression estimated baseline phase appears reasonable within

with some similarity within the brain to the sample angular mean estimates in Figure 5d but extremely unreasonable outside the brain. Also note that the ordinary least squares simple linear regression estimated task coefficients in Figure 5f appear unreasonable outside the brain and extremely unreasonable inside the brain near the [-π,π] boundary where there are phase transitions as in all fMRI phase data.

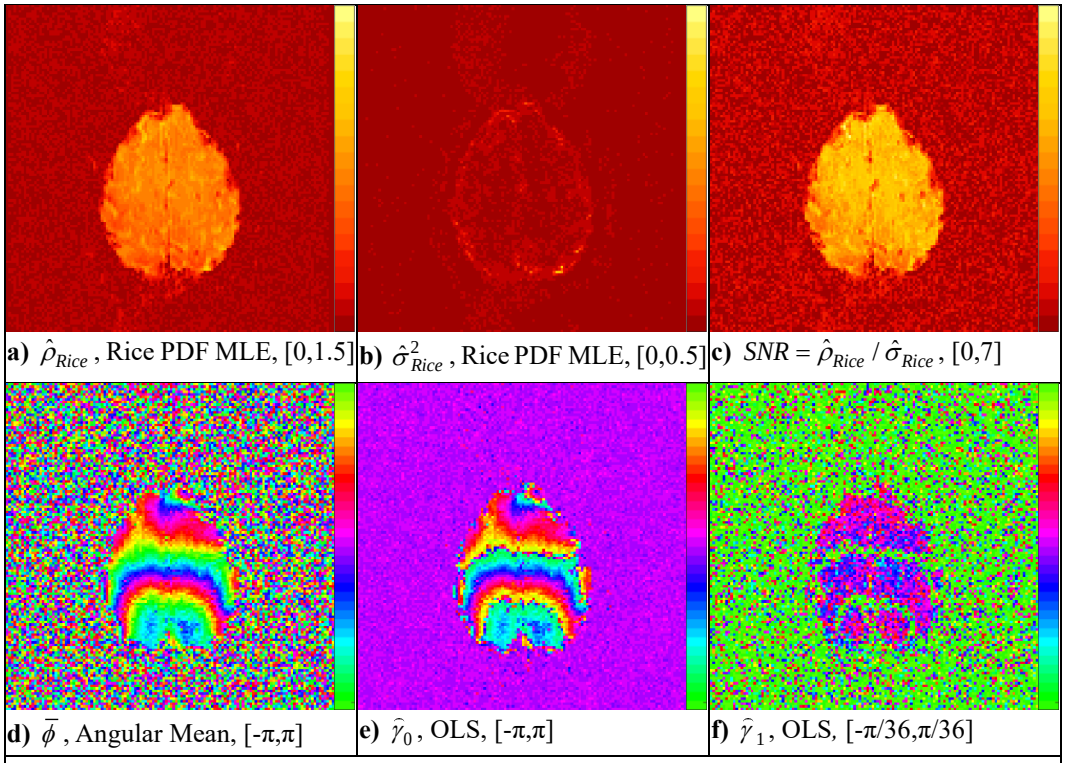

a) $\hat{\rho}_{Rice}$, Rice PDF MLE, [0,1.5] **b)** $\hat{\sigma}^2_{Rice}$, Rice PDF MLE, [0,0.5] **c)** $SNR = \hat{\rho}_{Rice} / \hat{\sigma}_{Rice}$, [0,7]

d) $\bar{\phi}$, Angular Mean, [-π,π] **e)** $\hat{\gamma}_0$, OLS, [-π,π] **f)** $\hat{\gamma}_1$, OLS, [-π/36,π/36]

Figure 5: Images of experimental data parameter estimates not from phase distribution.

In Figure 6 are voxel-wise estimates of parameters that do use Equation 5. In Figure 6a are voxel-wise null hypothesis estimates of the baseline phase coefficient γ_0 from Equation 11. In Figure 6b are null hypothesis estimates of the variance σ^2 from Equation 11. In Figure 6d are alternative hypothesis estimates of the baseline phase coefficient γ_0 from Equation 11. Note the similarity of the alternative hypothesis estimates of the baseline phase in Figure 6d to the null hypothesis estimates in Figure 6a and the sample angular mean estimates in Figure 5d but not the simple linear regression estimates in Figure 5e. In Figure 6e are alternative hypothesis estimates of the variance σ^2 from Equation 11. Note the similarity between the alternative hypothesis variance estimates in Figure 6e to the null hypothesis estimates in Figure 6b and the Rice distribution maximum likelihood estimates in Figure 5b. In Figure 6c are alternative hypothesis estimates of the task phase coefficient γ_1 from Equation 11. Note the differences between the task-related phase coefficients in Figure 6c that uses the mathematically correct phase distribution to those in Figure 5f that use a simple linear regression model. In Figure 6f are signed likelihood ratio test z statistics from Equation 12 for task activation. Note the exciting task-related phase activations in Figure 6e in the left motor cortex for the unilateral finger tapping within the almost always discarded phase time series.

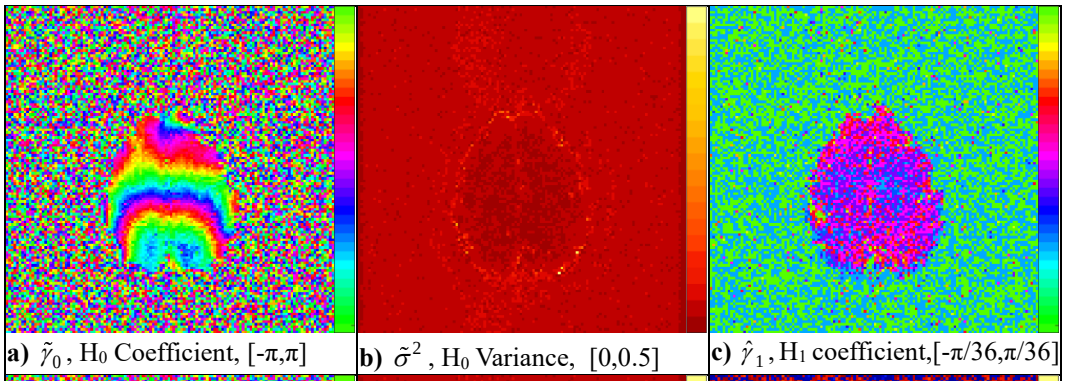

a) $\tilde{\gamma}_0$, H_0 Coefficient, [-π,π] **b)** $\tilde{\sigma}^2$, H_0 Variance, [0,0.5] **c)** $\hat{\gamma}_1$, H_1 coefficient,[-π/36,π/36]

d) $\hat{\gamma}_0$, H_1 Coefficient, [-π,π] **e)** $\hat{\sigma}^2$, H_1 Variance, [0,0.5] **f)** z, Test Statistic, [-7,7]

Figure 6: Images of simulated data MLE parameter estimates from phase distribution.

5. Conclusions

In fMRI, phase images and time series are rarely retained or analyzed. In rare instances where phase time series have been examined, it has been assumed that the marginal distribution of the phase was either normally distributed as in the high SNR scenario or approximated with the von Mises angular distribution and an arctangent link function. Here, the mathematically correct non-normal phase distribution was utilized which is valid at all *SNR*s. It was shown both in simulations and experimental fMRI data that the non-normal phase distribution works extremely well at all *SNR*s and has detected exciting task-related phase changes within experimental fMRI data in the left motor cortex from unilateral right-handed finger tapping. With this exciting breakthrough, phase activations from task related local magnetic field changes due to vascularity and direct neural current firing can be investigated.

References

1. Adrian DW, Maitra R, Rowe DB. Ricean versus Gaussian modelling in magnitude fMRI Analysis – Added Complexity with Few Practical Benefits. Stat, 2(1):303–316, 2013.

2. Adrian DW, Maitra R, and Rowe DB. Complex-valued time series modeling for improved activation detection in fMRI studies. Annals of Applied Statistics, 12(3):1451–1478, 2018.

3. Adrian DW, Maitra R, Rowe DB. Rice-Distributed Autoregressive Time Series Modeling and Improved Activation Estimation in FMRI Studies. Annals of Applied Statistics, 19(2):1494–1513, 2025.

4. Bandettini P, Jesmanowicz A, Wong E, Hyde J. Processing strategies for time-course data sets in functional MRI of the human brain. Magnetic Resonance in Medicine, 30:161–173, 1993.

5. Friston KJ, Jezzard P, and Turner R. Analysis of functional MRI time-series. Human Brain Mapping, 1:153–171, 1994.

6. Gudbjartsson H, Patz S. The Rician distribution of noisy data. Magnetic Resonance in Medicine 34(6):910–914, 1995.

7. Henkelman RM. Measurement of signal intensities in the presence of noise in MR images. Medical Physics, 12:232–233 1985. Erratum in Medical Physics, 13, 544,1986.

8. Johnson RA, Wehrly TE. Some angular-linear distributions and related regression models. Journal of the American Statistical Association, 1978;73(353):602–606.

9. Karaman MM, Nencka AS, Bruce IP, Rowe DB. Quantification of the Statistical Effects of Spatiotemporal Processing of Non-task fMRI Data. Brain Connectivity, 4(9):649-661, 2014.

10. Lai S and Glover GH. Detection of BOLD fMRI signals using complex data, Proceedings of the International Society for Magnetic Resonance in Medicine, p. 1671, 1997.

11. Lathi BP. Modern Digital and Analog Communication Systems. Ed. 3, Oxford University Press, p. 522, 1983.

12. Nencka AS, Hahn AD, Rowe DB. A Mathematical model for understanding the statistical effects of k-space (AMMUST-k) preprocessing on observed voxel measurements in fcMRI and fMRI. Journal of Neuroscience Methods, 181(2):268–282, 2009.

13. 1Rice SO. Mathematical analysis of random noise. Bell System Technological Journal, 23:282, 1944.Rowe DB, Logan, BR. A complex way to compute fMRI activation. Neuroimage 23:1078–1092, 2004.

4. Rowe DB. Parameter estimation in the magnitude-only and complex-valued fMRI data models. Neuroimage, 24:1124–1132, 2005.

15. Sakitis CJ, Rowe DB. Bayesian merged utilization of GRAPPA and SENSE (BMUGS) for in-plane accelerated reconstruction increases fMRI detection power. Magnetic Resonance Imaging, 115:110252 (2025).

16. Severini TA. Likelihood Methods in Statistics. Oxford University Press, Oxford, UK, 2001.

17. Von Mises R. Uber die Ganzzahligkeit der Atomgewichte und verwandte Gragen. Physikalische Zeitschrift 19:490–500, 1918.

18. Wang Z, Rowe DB, Li X, Brown DA. A Fully Bayesian Approach for Comprehensive Mapping of Magnitude and Phase Brain Activation in Complex-Valued fMRI Data. Magnetic Resonance Imaging, 109:271–285, 2024.

19. Wilks SS. The large-sample distribution of the likelihood ratio for testing composite hypotheses. Annals of Mathematical Statistics. 9(1):60–62, 1938.

20. Yu CH, Prado R, Ombao HC, Rowe DB. A Bayesian Variable Selection Approach Yields Improved Brain Activation From Complex-Valued fMRI. Journal of the American Statistical Association, 113(524):1395–1410, 2018.